Machine learning-enabled graphene-based electronic olfaction sensors and their olfactory performance assessment 🆂 🎖

Shirong Huang ⓘ ; Alexander Croy ✉ ⓘ ; Antonie Louise Bierling ⓘ ; Vyacheslav Khavrus ⓘ ;
Luis Antonio Panes-Ruiz ⓘ ; Arezoo Dianat ⓘ ; Bergoi Ibarlucea ✉ ⓘ ; Gianaurelio Cuniberti ✉ ⓘ

Check for updates

View Online

Export Citation

Articles You May Be Interested In

E-noses: Smells like the future of sensors

Scilight (May 2023)

Quantum origins of molecular recognition and olfaction in drosophila

J. Chem. Phys. (November 2012)

An explicit electron-vibron model for olfactory inelastic electron transfer spectroscopy

J. Appl. Phys. (April 2019)

02 January 2025 11:54:10

Machine learning-enabled graphene-based electronic olfaction sensors and their olfactory performance assessment ⓕ ⓢⓒⓘ

Shirong Huang,[1] ⓘ�D Alexander Croy,[2,a] ⓘD Antonie Louise Bierling,[1,3] ⓘD Vyacheslav Khavrus,[4] ⓘD
Luis Antonio Panes-Ruiz,[1] ⓘD Arezoo Dianat,[1] ⓘD Bergoi Ibarlucea,[1,5,a] ⓘD and Gianaurelio Cuniberti[1,5,a] ⓘD

AFFILIATIONS

[1]Institute for Materials Science and Max Bergmann Center for Biomaterials, TU Dresden, 01062 Dresden, Germany
[2]Institute of Physical Chemistry, Friedrich Schiller University Jena, Helmholtzweg 4, 07743 Jena, Germany
[3]Department of Psychotherapy and Psychosomatic Medicine, Faculty of Medicine, TU Dresden, 01307 Dresden, Germany
[4]SmartNanotubes Technologies GmbH, Dresdner Str. 172, 01705 Freital, Germany
[5]Dresden Center for Computational Materials Science (DCMS), TU Dresden, 01062 Dresden, Germany

Note: This paper is part of the APR Special Topic on Volatile Organic Compounds and their Applications.
[a]Authors to whom correspondence should be addressed: alexander.croy@uni-jena.de; bergoi.ibarlucea@tu-dresden.de; and gianaurelio.cuniberti@tu-dresden.de

ABSTRACT

Olfaction is an evolutionary old sensory system, which provides sophisticated access to information about our surroundings. In particular, detecting the volatile organic compounds (VOCs) emitted during natural and artificial processes can be used as characteristic fingerprints and help to identify their source. Inspired by the biological example, artificial olfaction aims at achieving similar performance and thus digitizing the sense of smell. Here, we present the development of machine learning-enabled graphene-based electronic olfaction sensors and propose an approach to assess their olfactory performance toward VOCs. Eleven transient kinetic features extracted from the sensing response profile are utilized as their fingerprint information. By mimicking the Sniffin' Sticks test, electronic olfaction sensors exhibit high olfactory performance toward four VOC odors (clove, eucalyptus, lemon, and rose scent) in terms of odor detection threshold, odor discrimination, and identification performance. Upon exposure to binary odor mixtures, response features of electronic olfaction sensors behave more similarly to that of an individual odor, with a tendency that correlates with their ratio, resembling the overshadowing effect in human olfactory perception. Molecular dynamics simulations and density functional theory calculations results reveal competing adsorption mechanisms between odorant molecules and sensing materials. This may facilitate electronic olfaction sensor applications in some emerging fields, such as environmental monitoring or public security.

I. INTRODUCTION

Olfaction, as one of the oldest senses in terms of evolution, provides a highly adapted way of gathering information about the chemical environment.[1] Detection and identification of volatile organic compounds (VOCs) are important tasks fulfilled by biological olfactory systems for navigation and survival.[2,3] In the context of modern-day applications, digitizing the sense of smell using micro- and nanoelectronic devices to identify VOCs and their mixtures results in bioinspired artificial olfaction.[4,5] The effectiveness of artificial olfaction, i.e., electronic noses (e-noses), relies on the one hand on the sensor hardware and on the other hand on the processing of the obtained signals. Herein, e-noses refer to instrumental replicas of the human sense of smell, comprising an array of electronic chemical sensors with partial specificity and a suitable pattern-recognition system, capable of detecting simple or complex odors.[6,7] Over the years, artificial olfaction has led to developments in biological modeling,[8] sensor technology,[9–11] and bioinspired technologies.[12,13] In this context, machine learning techniques are crucial to extract characteristic information and to provide means of VOC discrimination and identification.[14]

Over the past decades, there has been notable progress in the development of gas sensors for e-nose systems, including the PEN3 type portable electronic nose by AIR SENSE Analytics GmbH (Germany) and Mk3.3 by E-Nose Pty Ltd. (Australia). These sensors show great potential in a wide range of applications.[15–19]

Despite this significant progress, the compactness of e-noses remains a challenge due to the complex layout design of sensor arrays and the need for high working temperatures. Metal-oxide-semiconductor (MOS-type) gas sensors are a prominent type due to their low cost, feasible fabrication, and sensitivity.[20,21] However, they require high operating temperatures in the range of 200–500 °C since thermal energy is essential to activate the adsorption of ionized oxygen species and to overcome the barriers of sensing reactions. For example, the BME688 product by Bosch Sensortec (Germany) is a four-in-one gas sensor that includes artificial intelligence and is housed in a rugged yet compact $3.0 \times 3.0 \times 0.9 \, mm^3$ package, with an operating temperature of up to 320 °C. Accordingly, a heater has to be taken into consideration in the design of the sensor device.[22]

Carbon nanomaterials, such as carbon nanotubes and graphene, offer a promising alternative sensing material, due to their exceptional properties.[23,24] For example, SmartNanotubes GmbH (Germany) has produced carbon nanotubes-based electronic noses consisting of multi-channel sensors for various gases and VOC discrimination.[23,25] Graphene possesses remarkably high electron mobilities and an ultra-high surface-to-volume ratio,[26] and has already demonstrated outstanding performance in gas sensing applications compared to traditional materials, including high sensitivity, excellent reversibility, and low operation temperature (usually room temperature).[24,27,28] Therefore, the development of compact and miniaturized e-noses operated at room temperature is of significant importance.

Human olfactory performance can be evaluated using a specialized psychophysical test, such as the Sniffin' Sticks test (Burghardt®, Wedel, Germany), which was introduced by Hummel *et al.* in 1997 and has since been validated in multiple European countries.[29] This provides a semi-objective measure of olfactory function by presenting odor-filled felt pens to the subject. The assessment comprises three subtests: odor threshold (OT), odor discrimination (OD), and odor identification (OI).[30] To conduct the odor threshold (OT) test, the threshold concentration at which the subject can identify the odor (either 2-phenylethanol or n-butanol) is determined using a single-staircase based on three-alternative forced choice (3-AFC) procedure, beginning with a 4% solution (with scores ranging from 1 to 16). For the odor discrimination (OD) test, the subject is asked to identify the odor pen that has a different scent from a triplet that contains two identical odors and a different one, using a 3-AFC paradigm (with scores ranging from 0 to 16). In the odor identification (OI) test, the subject is required to identify the odor pen and indicate its name from a list of four written descriptors (with scores ranging from 0 to 16).[31] An overall score [TDI (Threshold score, Discrimination score, Identification score)] is then calculated by adding up the scores from the OT, OD, and OI tests. A score of 30.5 points or higher indicates normosmia, while a score between 16.5 and 30 points indicates hyposmia, and a score lower than 16.5 points indicates functional anosmia.[32] However, to the best of our knowledge, there have been no attempts to develop an olfactory performance assessment methodology for artificial olfaction.

In this contribution, we present the development of machine learning-enabled graphene-based single-channel electronic olfaction (e-olfaction) sensors and propose a methodology to evaluate their olfactory performance. We selected four VOC-based odors, namely, eucalyptol (Euca, eucalyptus scent), 2-nonanone (2Nona, lemon scent), eugenol (Euge, clove scent), and 2-phenylethanol (2Phe, rose scent), which are widely used in human olfactory performance assessment.[30] We achieved a low odor detection limit of 4.4 ppm (for 2Phe), and our e-olfaction platform showed high odor discrimination (83.3%) and identification (97.5%) accuracies. Moreover, we investigated the similarity of perceived features between binary odor mixtures and individual odors using e-olfaction. We also used molecular dynamics simulations (MDS) and density functional theory (DFT) calculations to elucidate the adsorption interaction between odorant molecules and sensing materials. Finally, we provide insights on the effect of humidity in the performance of the method and validate it by identifying additional VOCs more commonly tested in gas sensing applications using humid air as carrier gas. Our results demonstrate that the developed e-olfaction exhibits high olfactory performance in sniffing out VOC-based odors. This technology could be applied in various domains, such as environmental monitoring and public security.

II. RESULTS AND DISCUSSION
A. E-olfaction platform

The workflow of our developed e-olfaction platform is illustrated in Fig. 1, which consists of three steps: olfactory performance measurement, odor feature extraction, and odor TDI performance analysis. The essential component of this platform is the sensor device, which is built using a graphene dispersion prepared by exfoliation of graphite assisted with an 8-aminopyrene-1,3,6-trisulphonic acid trisodium salt (APTS) in an aqueous solution. While the usual approach for graphene sensor functionalization with pyrene derivatives relies on its modification after the deposition step,[33] here the exfoliation and functionalization take place at the same time.[34] APTS, therefore, plays a dual role as a stabilizer to preserve graphene dispersion and as active adsorption sites for analyte molecules.[24] The microelectrodes are bridged through graphene flakes via dielectrophoresis (DEP) of drop-cast graphene dispersion under an alternating current (AC), resulting in a chemiresistor-type gas sensor. The odor sensing measurement setup consists of three modules: an odor vapor generation module, an odor sensing measurement module, and an external signal displaying module. Individual odor tests mimicking Sniffin' sticks tests and binary odor mixture tests are conducted as shown in Fig. 1(a).

The raw data acquired from the odor sensing setup were the sensor current evolution of a single graphene-based gas sensor as a function of the operation time, comprising 24 repetitions for each odor (Euca, Euge, 2Phe, and 2Nona). The repetitions were performed to collect as much raw data as possible for machine learning in the subsequent steps. In a practical application, one repetition is sufficient for detection analysis once the machine learning classifier model has been established and deployed on the e-olfaction platform. In this work, instead of steady-state features, eleven transient features (a_1, b_1, c_1, a_2, b_2, c_2, S, k_{max}, k_{min}, a_{min}, and $Area$) extracted from sensing response profile are considered for machine learning analysis as shown in Fig. 1(b). The exponential features (a_1, b_1, c_1, a_2, b_2, and c_2) are fitting parameters extracted from sensing response profiles and sensing recovery profiles following exponential fitting, respectively. Transient feature S is the transient-state sensing response in the odor exposure phase, while feature $Area$ is the area under the sensing response curve
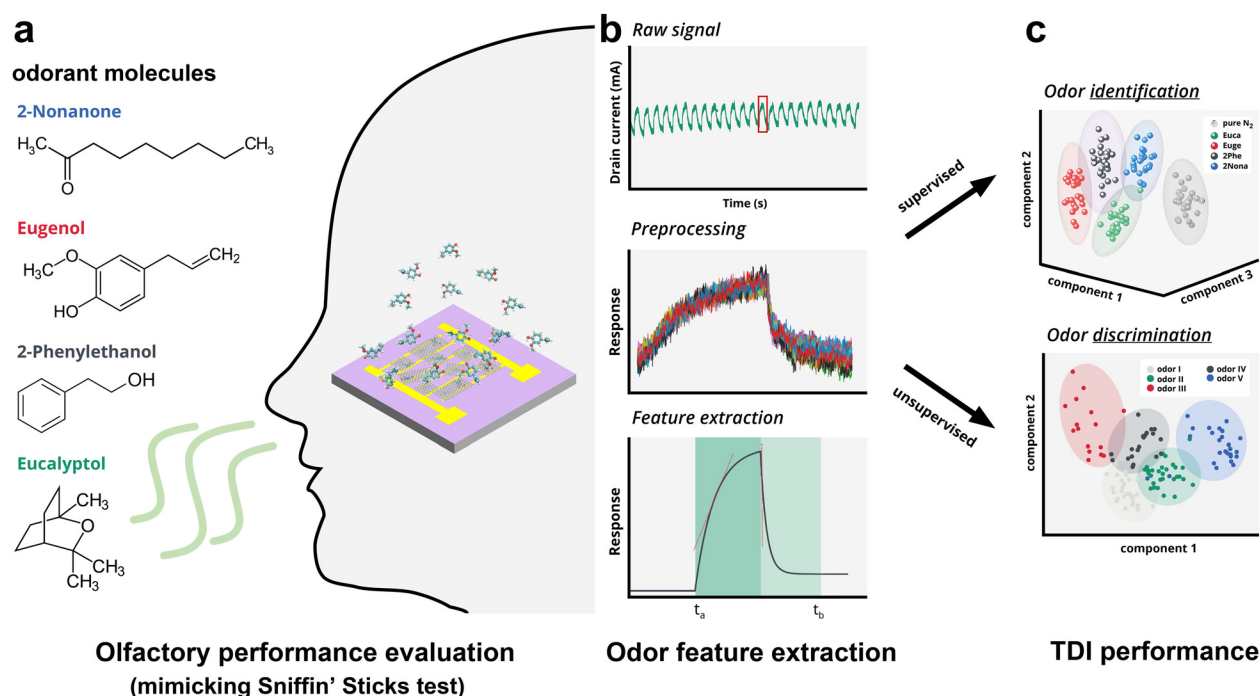
FIG. 1. E-olfaction platform. (a) Olfactory performance measurement. Odorant molecules are vaporized by the carrier gas (N_2) via a bubbling approach and delivered to the gas sensing test chamber for olfactory performance evaluation by mimicking the Sniffin' Sticks test. Four odorant molecules are involved, including 2-Nonanone (2Nona), Eugenol (Euge), 2-Phenylethanol(2Phe), and Eucalyptol(Euca), which are widely utilized to evaluate the olfactory performance of Anosmia patients in Sniffin' Stick tests. Odorant molecules reach the sensor device surface and interact with the active sensing materials (i.e., functionalized graphene) via physical/chemical adsorption. Charge transfer occurs between odorant molecules and sensing materials, altering the electrical conductivity of sensing materials. (b) Odor feature extraction. The electrical signal for each odor is then processed, including drift correction, signal normalization, feature extraction, etc. Each odor is represented by a multivariate feature vector. (c) Odor TDI results analysis. Finally, the olfactory performance of the e-olfaction platform is evaluated in terms of odor threshold (OT), discrimination (OD), and identification (OI) performance by machine learning.

in both odor exposure phase and odor flushing periods. Transient features k_{max} and k_{min} represent the maximum and minimum values existing in the sensing response profile following the first-derivative fitting transformation, while a_{min} represents the minimum value in the transformed sensing response profile following the second-derivative fitting transformation. The details on the feature extraction method are described in the supplementary material. Following features extraction, both unsupervised machine learning analysis and supervised machine learning analysis are conducted by mimicking the Sniffin' sticks test. Finally, the olfactory performance of the developed e-olfaction platform, i.e., odor threshold performance, odor discrimination performance, and odor identification performance, is evaluated as shown in Fig. 1(c).

B. Odor threshold characterization

To conduct the odor threshold test, the e-olfaction sensor device was exposed to odor 2Phe at decreasing concentrations ranging from 19.0 to 4.4 ppm. The same measurement was performed for pure N_2 under identical conditions to establish as an odorless control group. Odor clustering results by unsupervised machine learning (principal component analysis, PCA) are shown in Fig. 2. At high concentrations of odor 2Phe, such as 19.0 ppm, the odor 2Phe cluster and the reference cluster are clearly separated with a relatively large centroid

distance. However, as the concentration of odor 2Phe decreased to 15.8 ppm, its cluster overlapped with the reference cluster in several points. At the lowest concentration (4.4 ppm, the minimum value achieved by our setup), these two clusters exhibit moderate overlap. These results suggest that the developed e-olfaction platform can discriminate odor 2Phe from the odorless reference even at low concentrations, down to 4.4 ppm.

C. Odor discrimination characterization

In order to conduct the odor discrimination test, the e-olfaction sensor was exposed to individual odors, involving Euca, 2Nona, Euge, and 2Phe (pure N_2 as odorless reference). As defined by Sniffin' Sticks test, for odor discrimination, the subject has to indicate the different odor pen in a triplet without odor label information. Therefore, unsupervised machine learning (e.g., PCA, K-Means) was employed to discriminate different odors without odor label feeding. PCA is a nonparametric statistical technique primarily utilized for dimensionality reduction or compression of a high-dimensional dataset onto a lower-dimensional feature subspace to maintain most of the relevant information.[35] Following feature extraction and feature processing, the first two principal components of the odor features were plotted (PC1 vs PC2) as illustrated in Fig. 3(a). The first principal component explains 50.63% of the variance, and the second principal component explains
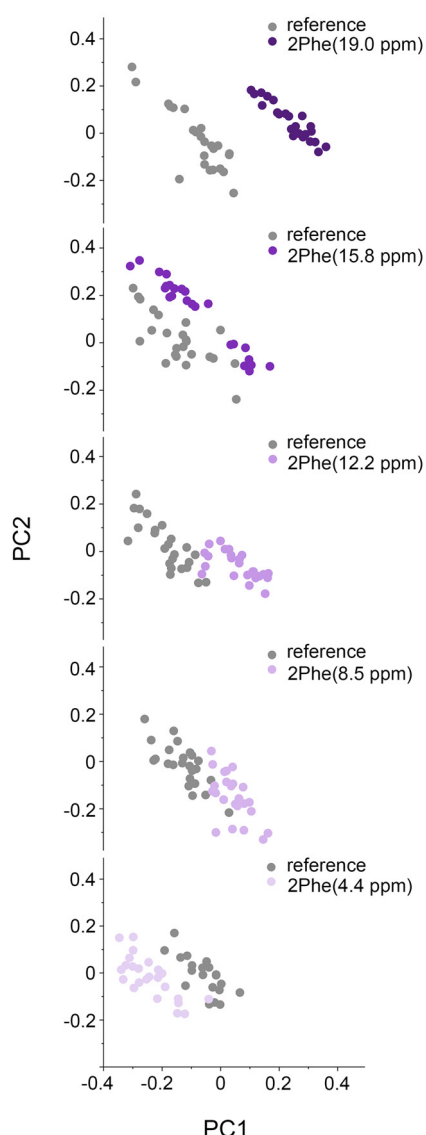
FIG. 2. Odor threshold performance. Discrimination of odor 2Phe from the odorless reference (pure N2) in principal component analysis (PCA) space with descending concentrations of odor 2Phe (from 19.0 to 4.4 ppm).

22.76%. Together, the first two principal components explain 73.39% of the variance. It is noticed that the 2Nona cluster demonstrates excellent separation from the other odor clusters, whereas the 2Phe, Euge, and Euca clusters exhibit some overlapping.

Meanwhile, odor clustering analysis by the K-Means algorithm (n_clusters = 5) was performed as illustrated in Fig. 3(b). Clustering analysis attempts to group similar results based on a similarity measure, among which distance functions, such as Euclidean distance,[36] are commonly utilized. Clusters are organized in such a fashion that any two samples within the same cluster have a minimal distance and any two samples across different clusters exhibit maximal distance.[37] Herein, the most popular clustering algorithm, i.e., the K-means

algorithm, is demonstrated as an example, and the results are shown in Fig. 3(b). The odor confusion matrix achieved by the K-Means algorithm is shown in Fig. 3(c). Based on the confusion matrix results, the discriminating precision result for each odor is analyzed.[38] As shown in Fig. 3(d), it is revealed that 2Nona exhibits the highest discriminative precision (95.8%) while Euca exhibits the lowest one (67.7%). Therefore, implementing the K-Means clustering algorithm, the average discriminative precision for all odors approaches 83.3%.

D. Odor identification characterization

The Sniffin' Sticks test requires the subject to identify an odor pen and indicate its name from a list of written odor labels, which corresponds to supervised machine learning analysis. In this section, the measurement data are the same as the one used in Sec. IV E, but with the addition of odor category labels. The supervised learning technique (e.g., linear discriminant analysis) utilizes labeled datasets to train classifier algorithms that can classify or predict outcomes for unknown datasets.[39] Odor feature datasets as well as their labels are processed by the classifier model, such as linear discriminant analysis (LDA), which is a linear transformation technique for dimensionality reduction and a well-known classifier.[40] In contrast to PCA, LDA attempts to find a feature subspace that optimizes class separability. Odor classification results are illustrated in Fig. 4(a). The first three linear discriminants account for the total variance (LD1, LD2, and LD3 explain 82.42%, 14.36%, and 2.67%, respectively). These results indicate that the four odor clusters, as well as the reference cluster, were classified accurately without confusion. With the 10-fold cross-validation approach,[41] the average classification accuracy by LDA classifier reaches 97.5% as shown in the supplementary material.

To assess the contribution of odor features to odor identification, the importance weight of these eleven feature parameters (a_1, b_1, c_1, a_2, b_2, c_2, S, k_{max}, k_{min}, a_{min}, and $Area$) were analyzed using the RandomForest classifier by scikit-learn software.[42] As depicted in Fig. 4(b), the four most important features (S, k_{max}, k_{min}, and a_{min}) makeup to 57.9% of total feature importance. The sole feature k_{min} contributes to 21.4% of total feature importance. Hence, these transient derivative features (S, k_{max}, k_{min}, and a_{min}) are discriminative for odors, constructing unique fingerprints (see supplementary material). The contribution of features whose importance weight is less than 5% (e.g., a_2, c_1, and c_2) is also essential to the effective odor identification as we could observe slight odor clusters overlapping following removing these small weight features (see supplementary material).

E. Electronic perception to binary odor mixture

In addition to the individual odors, the response toward binary odor mixtures is investigated as well. Details on the sampling protocols and measurements are described in the supplementary material. Following feature extraction, the feature data of odor mixtures are analyzed by PCA. As shown in Fig. 5(a), the first six principal components of a binary odor mixture could explain nearly 100% variance, while the first two principal components could explain more than 75%. The PCA score plot of a binary odor mixture, such as odor Euca-2Nona, is shown in Fig. 5(b). We found that the pure 2Nona cluster is separated very well from the pure Euca cluster without any overlapping. With the increasing Euca:2Nona ratio, the odor mixture cluster tends to move toward the pure Euca cluster and vice versa.
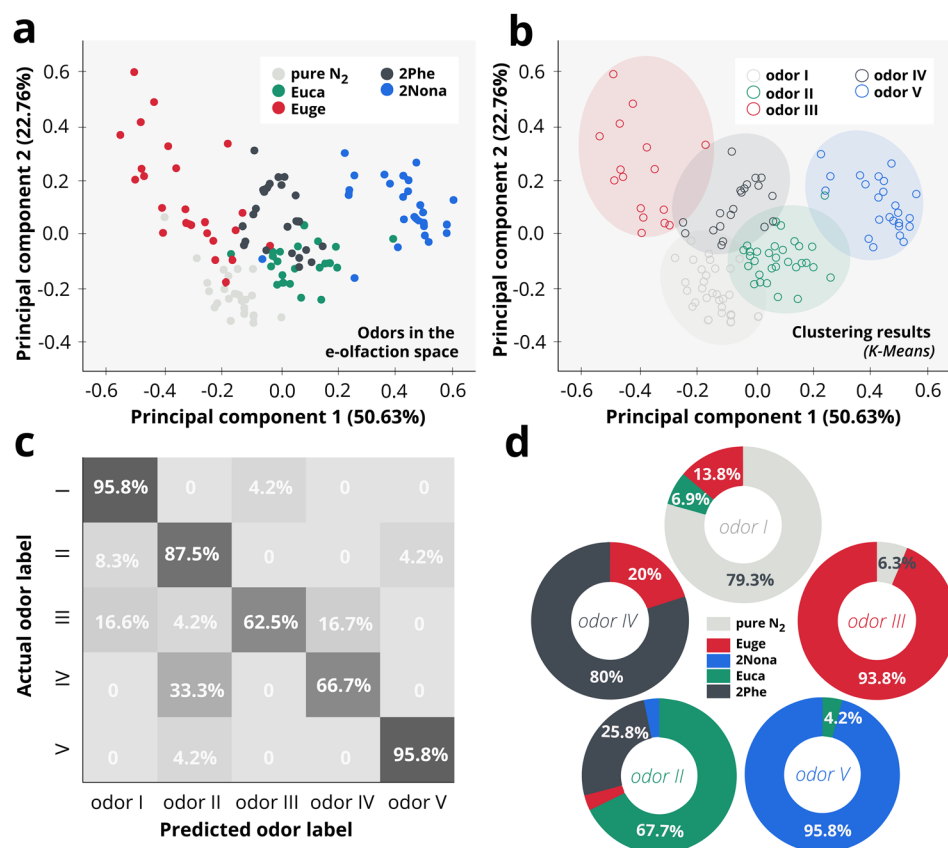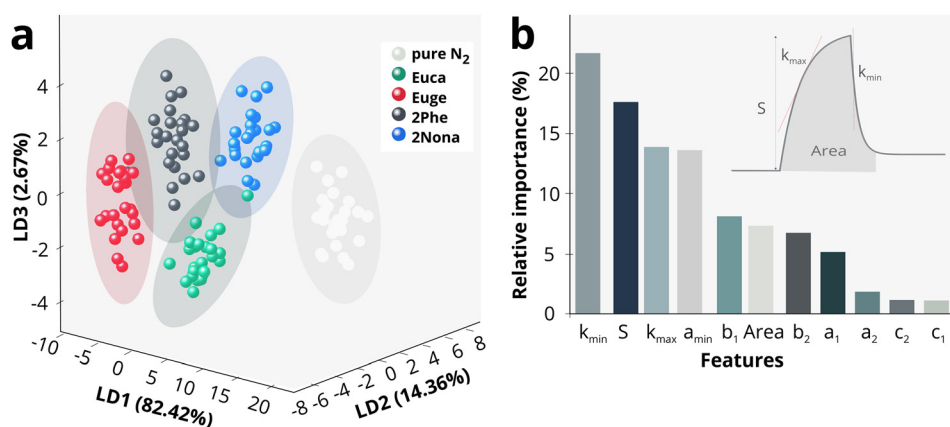
FIG. 3. Odor discrimination performance. (a) First principal component (PC1) vs second principal component (PC2) plot of odor clusters (ground truth in legend). (b) Odor clustering results implemented with the K-Means clustering algorithm (predicted label in legend). (c) Confusion matrix of odor clustering implemented with K-Means clustering algorithms. (d) Discrimination precision results of odor clustering implemented with the K-Means clustering algorithm. Color code: Euca (green), Euge (red), 2Phe (dark grey), 2Nona (blue), and reference (light gray).

Furthermore, a more quantitative analysis of the odor mixture features is carried out as schemed in Fig. 5(d). The centroid points of individual odor clusters and odor mixture clusters are obtained first, and the Euclidean distance between the centroid point of an odor-mixture cluster and the centroid point of a pure-odor cluster are measured in PCA space. Consequently, each odor mixture has two distance parameters, d_1 and d_2, and are represented in a 2D coordinate system (d_1 vs d_2), as illustrated in Fig. 5(e). A statistical result

based on the introduced concept of "probability," derived from the equations at the bottom panel of Fig. 5(d), is shown in Fig. 5(g). These results suggest that the features of the odor mixture Euca-2Nona behave closer to Euca, with a higher probability and certainty of finding Euca molecules in the mixture when its proportion in the mixture increases. A similar observation is found for the binary odor mixture Euge-2Phe, as shown in Figs. 5(c), 5(f), and 5(h), while odor Euge prevails in the perceived features over odor 2Phe. To sum up, Euca

FIG. 4. Odor identification performance. (a) Odor classification results implemented with a Linear Discriminant Analysis (LDA) classifier algorithm, the first three discriminants (LD1, LD2, LD3) explain over 99% variance. (b) Relative importance loadings of 11 features for the odor identification implemented with the random forest algorithm.
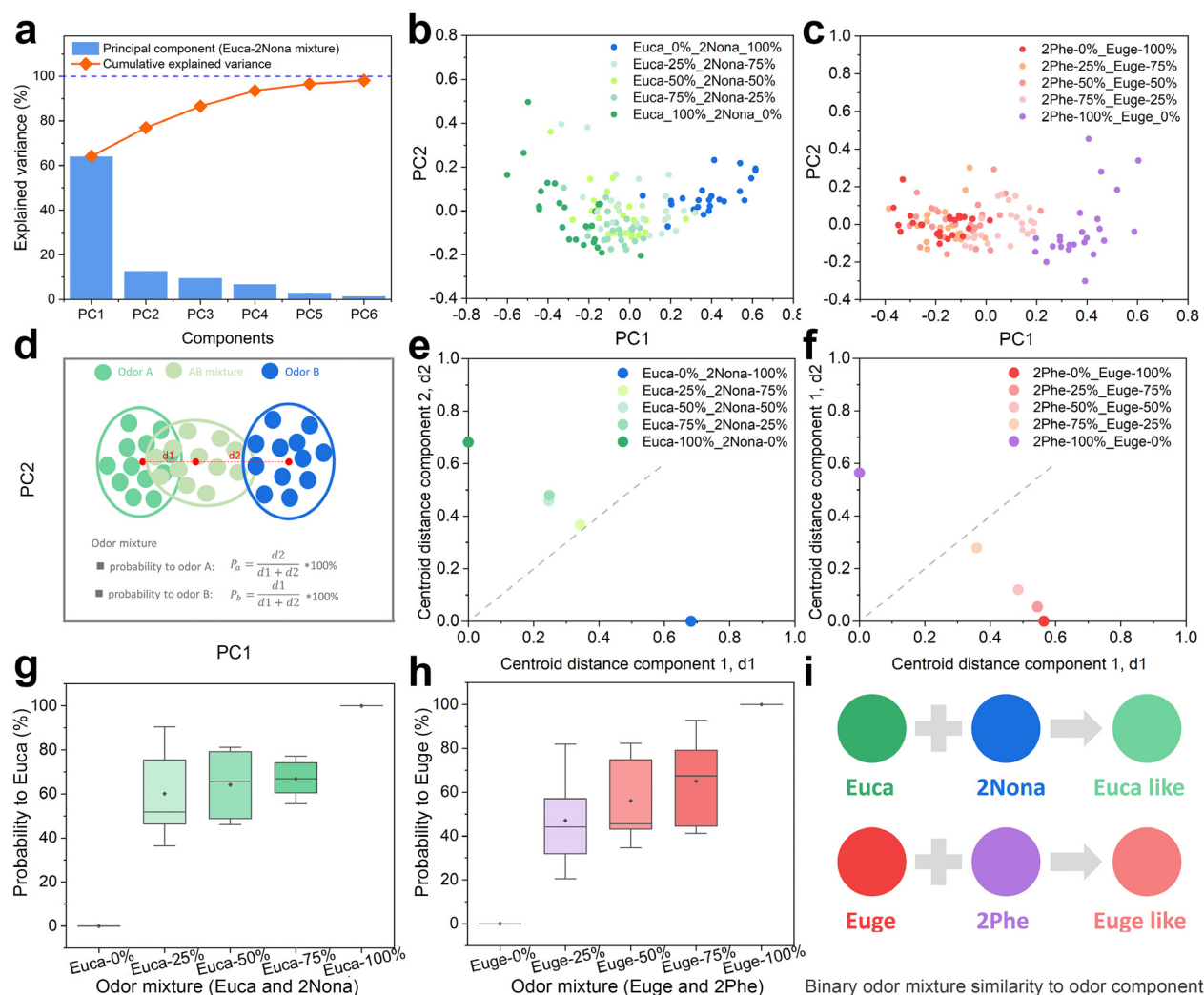
FIG. 5. Feature similarity of binary odor mixture to individual odor. (a) Explained variance of the first 6 principal components of a binary odor mixture (Euca and 2Nona) features and their cumulative explained variance. PCA score plots of binary odor mixtures (b) Euca and 2Nona, (c) Euge and 2Phe. (d) Schematic diagram of centroid distance component and similarity formula of binary odor mixture to odor component. d_1, centroid distance component 1, denotes centroid distance of odor mixture cluster and odor component 1 cluster. d_2, centroid distance component 2, denotes centroid distance of odor mixture cluster and odor component 2 cluster. Centroid distance component analysis plot of binary odor mixtures (e) Euca and 2Nona, (f) Euge and 2Phe. (g) Similarity of binary odor mixture Euca and 2Nona to odor component Euca. (h) Similarity of binary odor mixture Euge and 2Phe to odor component Euge. (i) Feature perception of binary odor mixture generated by the e-olfaction platform.

dominates the feature perception in the mixture Euca-2Nona, while Euge dominates the feature perception in the mixture Euge-2Phe as summarized in Fig. 5(i).

Previous human psychophysical studies reported that the perception of a binary odor mixture could give rise to one of these three outcomes: an elemental perception, a configural perception, or an overshadowing effect.[43,44] An elemental perception implies that both components of the odor mixture are perceived in the odor mixture, whereas a configural perception infers that a new odor is perceived.[45] Overshadowing refers to recognizing only one odor component in a binary mixture.[46] Hence, our developed e-olfaction sensor perceives features closer to one of the odor components in the mixture upon

exposure to binary odor mixtures, behaving similarly to the overshadowing effect in human olfaction perception.

F. Odorant molecules interaction with sensing materials

To provide insights on the underlying mechanism of the "overshadowing effect" perceived by the e-olfaction sensor, the interaction between odor molecules and APTS-functionalized graphene was investigated via classical molecular dynamics simulations (MDS) and density functional theory (DFT) calculations (see Sec. IV for details). Pure odor models consisting of Euca, 2Nona, Euge, 2Phe, and

odor mixture models, including Euca-2Nona, Euge-2Phe, Euca-Euge, Euca-2Phe, Euge-2Nona, and 2Nona-2Phe, were simulated. All models contained the same amount of odor molecules. The morphology of odor molecules on the graphene surface is demonstrated in Figs. 6(a)–6(f). The center-of-mass (COM) distance between odor molecules and APTS molecules is measured and shown in Fig. 6(g). Binding energy and charge transfer amount between odor molecules and APTS molecules were calculated by DFT and are illustrated in Figs. 6(h) and 6(i), respectively.

In the individual odor case shown in Figs. 6(a) and 6(b), odor molecules of both Euca and 2Nona favor surrounding APTS. The heads of odor molecules, which contain oxygen functional groups, prefer to point into APTS, which is mainly governed by traditional dipole–dipole interaction.[47] In the odor mixture model shown in Fig. 6(c), we observed that Euca molecules approach APTS much closer than 2Nona, which is supported by the COM distance to APTS shown in Fig. 6(g). Comparing the odor mixture model with the pure odor model, the COM distance to APTS of odor Euca decreases while the COM distance to APTS of 2Nona increases, indicating competitive adsorption of Euca and 2Nona on APTS. The binding energy of Euca is slightly weaker than that of 2Nona, whereas the Euca molecule is smaller and more compact than 2Nona, which might be more beneficial for Euca to approach APTS closely.

Odor Euge and 2Phe exhibit very similar structures, consisting of a benzene ring and oxygen-containing functional groups. In the pure odor case shown in Figs. 6(d) and 6(e), similar to Euca and 2Nona, Euge and 2Phe molecules are found to surround APTS. The odor

molecules' heads are observed to point into the APTS head, which is mainly affected by hydrogen bonding interaction between the head of odor molecules and the head of APTS.[48] Hydrogen bonding interaction is believed to be stronger than conventional dipole–dipole interaction.[49,50] Apart from hydrogen bonding interaction, π–π stacking exists between Euge or 2Phe and APTS as well, which does not exist in the Euca or 2Nona model. For this reason, some Euge and 2Phe molecules are observed to stack onto APTS in Fig. 6(f). In the odor mixture model, the COM distance to APTS is demonstrated and compared with the pure odor model shown in Fig. 6(g). In the odor mixture model, the COM distance to APTS of Euge decreases a lot whilst the COM distance to APTS of 2Phe increases, which can be interpreted as competitive adsorption of Euge and 2Phe on APTS. This competitive adsorption originates from different binding energies to APTS, as depicted in Fig. 6(h). Euge's binding energies are larger than 2Phe's leading to solid binding between Euge and APTS. Consequently, Euge occupies more space near APTS than 2Phe.

Odor molecules interact with APTS-functionalized graphene involving two events: odor molecules adsorption on APTS and subsequently charge transfer between odor molecules and APTS-functionalized graphene. Both synergistically yield a characteristic sensing response.[51] The charge transfer amount between odor molecules and APTS-functionalized graphene is calculated by DFT, as shown in Fig. 6(i). Under the same circumstances, odor Euca transfers 18.4% more charge to APTS than 2Nona, while Euge transfers 83.8% more charge to APTS than 2Phe. With both odor adsorption and charge transfer in mind, odor molecules exhibiting stronger
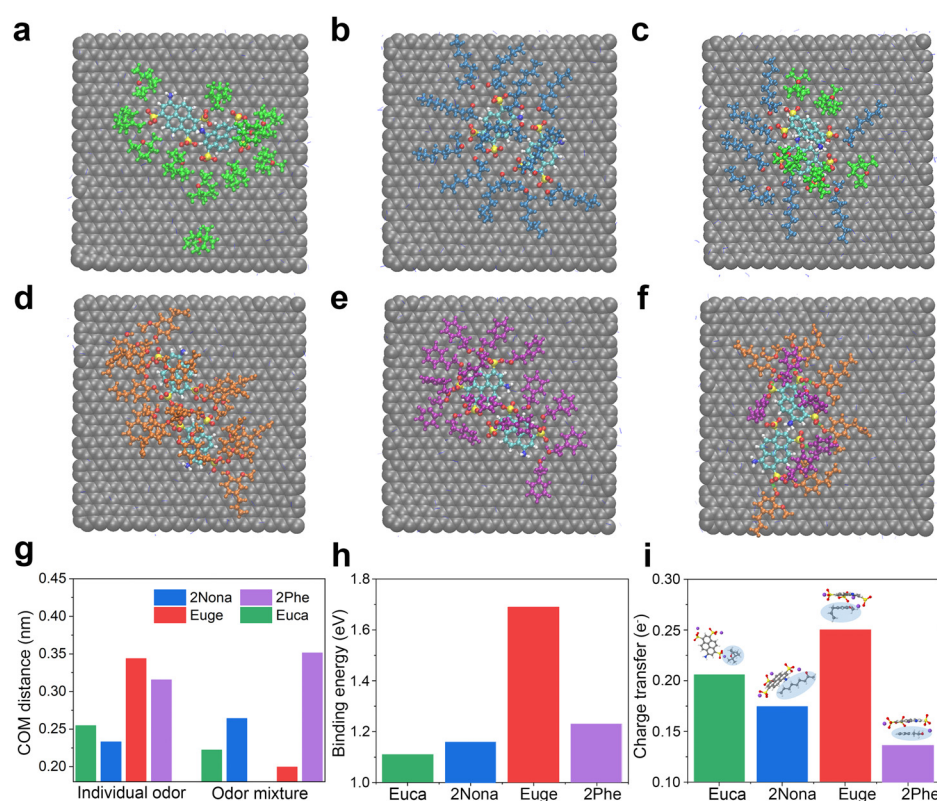
FIG. 6. Odorant molecule interaction with APTS functionalized graphene. Snapshot of odorant molecules interacting with APTS-functionalized graphene via molecular dynamics simulations, (a) Euca, (b) 2Nona, (c) Euca and 2Nona odor mixture, (d) Euge, (e) 2Phe, (f) Euge and 2Phe odor mixture. Color code: graphene (gray), Euca (lime), 2Nona (blue), Euge (orange), 2Phe (purple), carbon (cyan), nitrogen (blue), sulfur (yellow), oxygen (red). (g) Center of mass (COM) distance between odor molecules and APTS molecules in the context of individual odor and binary odor mixture, respectively. Binding energy (h) and charge transfer (i) between odorant molecules and APTS from DFT calculations.

interaction with sensing element materials embrace more chances to approach the functionalized graphene and dominate the signal characteristic in the odor mixture, which subsequently suppresses the signal of the other odor. These results demonstrate that owing to the distinct binding energies and charge transfer characteristics of odors, competitive adsorption to the sensing material occurs between two odor components in the mixture.

G. Impact of air and humidity

Hydrogen bonding interaction induced by humidity plays an important role in the gas sensing activities, particularly for graphene-based chemiresistive-type gas sensors, as it was verified in our previous work.[24] Although the humidity and presence of air may affect the intrinsic response, i.e., the interaction between the sensor and the target VOC, the effective response induced by such interaction is still distinct and, therefore, detectable by machine learning classifier algorithms. This could be verified by performing experiments using air as carrier gas and detecting VOCs and their binary mixture with water vapor. The experiment details, response results, as well as classification results are shown in the supplementary material.

First, ethanol (ETH) was chosen as a frequently found VOC in gas sensor applications. The sensor was exposed to 48 cycles of pure water (alcohol by volume 0 or ABV0), pure ethanol (ABV100), and a binary mixture of 80% ethanol and 20% water (ABV80). The pure ethanol cluster is very well separated from the other clusters. The water vapor and binary mixture have a very small degree of overlapping, allowing for their classification. The overall classification accuracy to identify these three vapors could reach 91.7%. From these results, we can conclude that the extracted features (fingerprint) from the effective sensing response profile are distinct. In combination with machine learning algorithms, these multiple transient features could contribute to the VOC identification at high accuracy.

We further proceeded to the exposure of four additional common VOCs, namely, ethanol (ETH), methanol (MTH), 2-propanol (PRL), and water vapor. In the PCA analysis, it could be found that the first three components could explain around 87.7% variance. The water vapor cluster and methanol vapor cluster were well separated from the other two, while the ethanol cluster and 2-propanol cluster showed some overlapping. With the LDA, the separability of these four clusters was better except for a small overlapping between ethanol and 2-propanol. With the excellent separability in LDA space, the confusion matrix of these gases' classification exhibited high accuracy (see supplementary material). The overall classification accuracy was 95.8% implemented by the hold-out strategy, in which 75% of features were employed to train classifier models and the rest features were employed to validate the trained classifier models. These experiments suggest that the discrimination of VOCs using multiple transient features is effective in ambient air and not just using nitrogen as carrier gas.

An aging test by exposing the sensor to various humidity levels for 36 h (720 cycles) did not evidence sensor deterioration due to water vapor effects.

III. CONCLUSION

In this work, we introduce the development of machine learning-enabled graphene-based single-channel electronic olfaction (e-olfaction) sensors, along with an olfactory performance assessment methodology for characterizing their performance. The e-olfaction sensor device comprises a single-channel nanosensor, which distinguishes it from conventional e-nose systems that utilize sensor arrays, and operates at room temperature. This unique design shows great potential for miniaturization and portability. We extract eleven kinetically transient-state features are extracted from odor sensing response profiles, which takes advantage of characteristic response profiles of odor sensing. Our e-olfaction concept exhibits excellent performance under controlled lab conditions, not limited by the use of air as the carrier gas, in terms of odor threshold, odor discrimination and odor identification. Specifically, we achieve a low odor threshold toward 2Phe (4.4 ppm) and an excellent odor discrimination performance (83.3%). Furthermore, the incorporation of supervised machine learning classifier algorithms (LDA) enables high odor identification accuracy (97.5%). Simultaneously, the e-olfaction device manifests efficient processing capability toward binary odor mixtures. The response to binary odor mixtures is shown to behave close to an individual odor while the response of the other odor is partially suppressed. This phenomenon is analogous to the overshadowing effect in human olfaction perception upon processing binary odor mixtures.

The relatively long sampling data acquisition period is a limitation of this work, which could be addressed by optimizing the sampling protocols and developing faster responding sensing materials. Future investigations could explore this topic, which is out of the scope of the present work.

The potential compact size of our e-olfaction platform meets the miniaturization requirements for seamless integration into various devices. It leverages arrays of highly sensitive nanomaterials functionalized in diverse ways, thereby enabling the detection and discrimination of a much larger amount of target odor molecules and their complex mixtures. When coupled with mobile devices for data analysis, it holds great promise for assisting individuals with olfactory disorders in the near future. In addition, it has the potential to be applied in numerous emerging fields, such as environmental monitoring or public security.

IV. METHODS

A. Graphene dispersion preparation

Graphite powder (crystalline, $-20 + 84$ mesh, 99.9%, metal basis, CAS: 7782-42-5) was ordered from Alfa Aesar Company. 8-Aminopyrene-1,3,6-trisulphonic acid trisodium salt (APTS, $C_{16}H_8NNa_3O_9S_3$, CAS: 196504-57-1) was bought from VWR International Company. The optimized recipe for graphene dispersion preparation was as below: 5 ml APTS aqueous solution (1 mg/ml) was mixed with 5 ml graphite powder aqueous solution (30 mg/ml), the mixture was then sonicated for 2 h by horn-type sonicator (50% amplitude, Model 250-D, Branson Digital Sonifier, U.S.) in an ice bath. Afterward, the obtained solution was left to stand overnight. To further remove unexfoliated graphite particles, the dispersions were centrifuged at 4000 rpm for 2 min (Eppendorf, MiniSpin plus, Germany), and the top 50% supernatant was pipetted out to another centrifugation tube. The rest was discarded. Following feeding deionized (DI) water to the original volume, the supernatant dispersion was then re-dispersed by a mild sonication setup (VWR ultrasonic cleaner, type: USC 300 TH, HF 45 kHz, 80 W, U.S.) for 10 min in an ice bath. Thereafter, the above centrifugation and re-dispersing

procedure were performed twice more. Finally, the aqueous dispersion of graphene functionalized by APTS was achieved.

B. Sensor device fabrication

The sensor device was fabricated by dielectrophoretic alignment of graphene flakes on gold interdigitated electrodes (IDEs) fabricated on silicon wafers. Electrode fabrication was done utilizing a standard microfabrication process comprising photolithography, gold thermal evaporation and liftoff, as introduced in our previous published work.[25] First, the IDEs pattern were fabricated on p-type Si substrate (4-in.) with 300 nm of thermally grown SiO_2 using photolithography techniques (MJB4, SÜSS MicroTec, Germany). 15 nm chromium and 100 nm gold were then deposited on the substrate via thermal evaporation and liftoff process. After that, the bare devices were cleaned with acetone and isopropanol, respectively. Finally, the devices were heated to $100\,°C$ for 5 min in order to remove residual solvents and naturally cooled down to room temperature. IDE structure on the device features a gap size of $3\,\mu m$ and a finger width of $4\,\mu m$, respectively. Alternating current DEP with a signal generator (AFG320 signal generator, Sony-Tektronix, Japan) was applied to deposit graphene on the device, which bridged neighboring electrodes precisely and achieved a homogeneous graphene network on the device. DEP parameters, including frequency of the applied signal (f), peak-to-peak voltage (V_{PP}), and processing time (t), play a major role in the alignment of graphene flakes.[52] The optimized parameters were as follows: Vpp = 10 V, f = 200 kHz, t = 30 s. In a typical DEP procedure, a droplet of $10\,\mu l$ dispersion was pipetted onto the IDE, which was fixed on a probe station (Karl Süss, Garching, Germany), then alternating current with specific frequency was applied on the sensor device for 30 s, followed by DI water rinsing and N_2 flow drying. Sensor device fabrication was completed and stored under an inert atmosphere (N_2) until use.

C. Odor vapor preparation

Four basic odors, eucalyptol (CAS number: 470-82-6, item number: C80601–500ML, purity ≥ 99.0%, Sigma-Aldrich, U.S.), 2-nonanone (CAS number: 821–55-6, item number: W278505-250G-K, purity ≥ 99.0%, Sigma-Aldrich, U.S.), eugenol (CAS number: 97-53-0, item number: W246700-1 KG-K, purity ≥ 98.0%, Sigma-Aldrich, U.S.), and 2-phenylethanol (CAS number: 60-12-8, item number: 77861-1L, purity ≥ 99.0%, Sigma-Aldrich, U.S.), were investigated in this work. A bubbler evaporation system was developed to generate odor vapor as well as deliver odor vapor to the gas chamber.[53] The flow rates of dry nitrogen, acting as carrier gas and dilution gas, were tuned by mass flow controllers (MFC, type number: GF040, Brooks Instruments Company). The source of both carrier gas and dilution gas was nitrogen, whose flow rate was precisely controlled by a mass flow controller (MFC). Odor concentration could be finely tuned by combining the flow rate of both carrier and dilution gas. For the analysis of the impact of humidity on the results, we substituted N_2 for ambient air as carrier gas. The bubbling approach using air through water and ethanol was used to generate their vapors at different ratios.

D. Odor sensing measurement

The sensing performance of e-olfaction toward both individual odor and odor mixture were evaluated at room temperature ($20\,°C$), respectively. The gas chamber was a homemade gas sensing setup and applied to measure the electrical property of the sensor upon exposure to individual odor vapor or odor mixture.[25] Upon odor vapor adsorbed by functionalized graphene on the sensor, the electrical conductivity of the sensor shifted due to the occurrence of charge carrier transfer between odor molecules and functionalized graphene. A constant voltage ($V = 0.1$ V) was applied to the sensor and the sensor current (I) was continuously recorded by a source meter (Keithley 2602, Tektronix GmbH, Germany) during exposure to odor vapors and recovery steps under pure nitrogen flow. Upon odor vapor adsorption by functionalized graphene on the sensor, the electrical conductivity of the sensor shifted due to the occurrence of charge carrier transfer between odor molecules and functionalized graphene. Following that, the path of carrier gas was switched off while the flow rate of dilution gas was increased to desorb and flush odor molecules from the graphene and released sensor recovery. In this work, the period for odor exposure and odor flushing is 15 and 10 min, respectively. To produce more data for machine learning analysis, 24 repetition tests were carried out for each odor test on the same condition. Before the initial cycle test, a stabilization process was performed to remove the adsorbed water or other contaminants was performed, in which pure nitrogen flow was active until the resistance of the sensor device approached a plateau state. In this work, a set of visual basic (VB) scripts were developed to automatically manage the whole measurement procedure,[54] including, start time and end time of the odor exposure step as well as odor flushing step, the flow rate of the carrier gas, and dilution gas in a different phase, as well as acquire current information, etc.

E. Odor discrimination

Odor discrimination aims to classify odor scatters with similar features into the same class while odor scatters with distinctive properties into different groups. This goal could be achieved via unsupervised machine learning. In this session, 4 odors, as well as an odorless reference (pure N_2), were discriminated. Before feeding into clustering algorithms, feature data of all odors had transformation preprocessing using StandardScaler, MinMaxScaler, and L2 normalization algorithms. The transformed features were further applied principal component analysis (PCA) for dimensionality reduction and analyzed with diverse clustering algorithms.

F. Odor identification

Odor identification is to predict the label information for the new odor from known labels after algorithm training. This could be achieved via supervised machine learning. In this session, 4 odors, as well as odorless reference (pure N_2), were identified with labels. In contrast to unsupervised machine learning, odor labels target had to be predicted as well.[39] All the features together with additional target (odor labels) information were split up into two sets, 75% data were used to train classifier algorithms while the rest 25% data were used to test classifier algorithms. Before the training data were fed into classifier algorithm, for example, linear discriminant analysis (LDA) algorithm, the features of the training dataset were transformed with StandardScaler algorithm. Afterward, the transformation parameters generated from training data were applied upon the test data set to generate transformed test data set. The prediction accuracy achieved by the LDA algorithm could be obtained. Meanwhile, the performance of LDA classifier algorithms was achieved using K-Fold

cross-validation ($K = 10$) approach. The above data processing of both unsupervised and supervised machine learning was conducted via a set of Python programs.

SUPPLEMENTARY MATERIAL

See the supplementary material for additional results, supporting data, and data analysis procedures.

AUTHOR DECLARATIONS
Conflict of Interest

The authors have no conflicts to disclose.

Author Contributions

Shirong Huang: Formal analysis (equal); Investigation (equal); Methodology (equal); Software (equal); Writing – original draft (equal). **Alexander Croy:** Conceptualization (equal); Data curation (equal); Funding acquisition (equal); Project administration (equal); Supervision (equal); Writing – review & editing (equal). **Antonie Louise Bierling:** Methodology (equal); Visualization (equal); Writing – review & editing (equal). **Vyacheslav Khavrus:** Investigation (equal); Methodology (equal). **Luis Antonio Panes-Ruiz:** Methodology (equal). **Arezoo Dianat:** Investigation (equal); Methodology (equal). **Bergoi Ibarlucea:** Conceptualization (equal); Data curation (equal); Funding acquisition (equal); Methodology (equal); Project administration (equal); Supervision (equal); Writing – review & editing (equal). **Gianaurelio Cuniberti:** Conceptualization (equal); Funding acquisition (equal); Project administration (equal); Supervision (equal); Writing – review & editing (equal).

DATA AVAILABILITY

The data that support the findings of this study are available from the corresponding authors upon reasonable request.

REFERENCES

[1]C. Sarafoleanu, C. Mella, M. Georgescu, and C. Perederco, J. Med. Life **2**(2), 196–198 (2009).

[2]N. Zannoni, M. Wikelski, A. Gagliardo, A. Raza, S. Kramer, C. Seghetti, N. Wang, A. Edtbauer, and J. Williams, Sci. Rep. **10**(1), 15879 (2020).

[3]T.-M. Koski, T. Laaksonen, E. Mäntylä, T. Ruuskanen, T. Li, P. S. Girón-Calva, L. Huttunen, J. D. Blande, J. K. Holopainen, and T. Klemola, Ethology **121**(12), 1131–1144 (2015).

[4]A. J. M. Barbosa, A. R. Oliveira, and A. C. A. Roque, Trends Biotechnol. **36**(12), 1244–1258 (2018).

[5]C. Ban, X. Min, J. Xu, F. Xiu, Y. Nie, Y. Hu, H. Zhang, M. Eginligil, J. Liu, W. Zhang, and W. Huang, Adv. Mater. Technol. **6**(11), 2100366 (2021).

[6]J. W. Gardner and P. N. Bartlett, Sens. Actuators, B **18**(1–3), 210–211 (1994).

[7]J. A. Covington, S. Marco, K. C. Persaud, S. S. Schiffman, and H. T. Nagle, IEEE Sens. J. **21**(11), 12969–12990 (2021).

[8]A. Sharma, R. Kumar, I. Aier, R. Semwal, P. Tyagi, and P. Varadwaj, Curr. Neuropharmacol. **17**(9), 891–911 (2019).

[9]J. Gutierrez and M. C. Horrillo, Talanta **124**, 95–105 (2014).

[10]S. Y. Park, Y. Kim, T. Kim, T. H. Eom, S. Y. Kim, and H. W. Jang, InfoMat **1**(3), 289–316 (2019).

[11]F. Rock, N. Barsan, and U. Weimar, Chem. Rev. **108**(2), 705–725 (2008).

[12]Y. A. Jodat, K. Kiaee, D. V. Jarquin, R. L. De la Garza Hernandez, T. Wang, S. Joshi, Z. Rezaei, B. A. G. de Melo, D. Ge, M. S. Mannoor, and S. R. Shin, Adv. Sci. (Weinheim, Ger.) **7**(5), 1901878 (2020).

[13]H. J. Ko and T. H. Park, J. Biol. Eng. **10**, 17 (2016).

[14]S. Huang, A. Croy, L. A. Panes-Ruiz, V. Khavrus, V. Bezugly, B. Ibarlucea, and G. Cuniberti, Adv. Intell. Syst. **4**(4), 2200016 (2022).

[15]F. S. Fedorov, A. Yaqin, D. V. Krasnikov, V. A. Kondrashov, G. Ovchinnikov, Y. Kostyukevich, S. Osipenko, and A. G. Nasibulin, Food Chem. **345**, 128747 (2021).

[16]H. Rottiers, D. A. T. Sosa, L. Van de Vyver, M. Hinneh, H. Everaert, J. De Wever, K. Messens, and K. Dewettinck, Food Anal. Methods **12**(2), 475–488 (2018).

[17]J. Zhang, Y. Xue, T. Zhang, Y. Chen, X. Wei, H. Wan, and P. Wang, J. Electrochem. Soc. **167**(14), 147519 (2020).

[18]A. Lichtenstein, E. Havivi, R. Shacham, E. Hahamy, R. Leibovich, A. Pevzner, V. Krivitsky, G. Davivi, I. Presman, R. Elnathan, Y. Engel, E. Flaxer, and F. Patolsky, Nat. Commun. **5**, 4195 (2014).

[19]B. Shan, Y. Y. Broza, W. Li, Y. Wang, S. Wu, Z. Liu, J. Wang, S. Gui, L. Wang, Z. Zhang, W. Liu, S. Zhou, W. Jin, Q. Zhang, D. Hu, L. Lin, Q. Zhang, W. Li, J. Wang, H. Liu, Y. Pan, and H. Haick, ACS Nano **14**(9), 12125–12132 (2020).

[20]M. M. Macias, A. G. Manso, C. J. Orellana, H. M. Velasco, R. G. Caballero, and J. C. Chamizo, Sensors (Basel) **13**(1), 208–220 (2012).

[21]E. Bonah, X. Huang, R. Yi, J. H. Aheto, R. Osae, and M. Golly, J. Food Process Eng. **42**(6), e13236 (2019).

[22]R. Kumar, X. Liu, J. Zhang, and M. Kumar, Nano-Micro Lett. **12**(1), 164 (2020).

[23]L. A. Panes-Ruiz, L. Riemenschneider, M. M. Al Chawa, M. Loffler, B. Rellinghaus, R. Tetzlaff, V. Bezugly, B. Ibarlucea, and G. Cuniberti, Nano Res. **15**, 2512–2521 (2021).

[24]S. Huang, L. A. Panes-Ruiz, A. Croy, M. Löffler, V. Khavrus, V. Bezugly, and G. Cuniberti, Carbon **173**, 262–270 (2021).

[25]L. A. Panes-Ruiz, M. Shaygan, Y. Fu, Y. Liu, V. Khavrus, S. Oswald, T. Gemming, L. Baraban, V. Bezugly, and G. Cuniberti, ACS Sens. **3**(1), 79–86 (2018).

[26]F. Yavari and N. Koratkar, J. Phys. Chem. Lett. **3**(13), 1746–1753 (2012).

[27]H. Hu, X. Yang, X. Guo, K. Khaliji, S. R. Biswas, F. J. G. de Abajo, T. Low, Z. Sun, and Q. Dai, Nat. Commun. **10**(1), 1131 (2019).

[28]W. Li, X. Geng, Y. Guo, J. Rong, Y. Gong, L. Wu, X. Zhang, P. Li, J. Xu, G. Cheng, M. Sun, and L. Liu, ACS Nano **5**(9), 6955–6961 (2011).

[29]T. Hummel, B. Sekinger, S. R. Wolf, E. Pauli, and G. Kobal, Chem. Sens. **22**(1), 39–52 (1997).

[30]T. Hummel, K. Rissom, J. Reden, A. Hahner, M. Weidenbecher, and K. B. Huttenbrink, Laryngoscope **119**(3), 496–499 (2009).

[31]M. Wolfensberger, I. Schnieper, and A. Welge-Lussen, Acta Oto-Laryngol. **120**(2), 303–306 (2000).

02 January 2025 11:54:10

[32]G. Kobal, L. Klimek, M. Wolfensberger, H. Gudziol, A. Temmel, C. M. Owen, H. Seeber, E. Pauli, and T. Hummel, Eur. Arch. Oto-Rhino-Laryngol. **257**(4), 205–211 (2000).

[33]D. K. H. Tsang, T. J. Lieberthal, C. Watts, I. E. Dunlop, S. Ramadan, A. E. del Rio Hernandez, and N. Klein, Sci. Rep. **9**(1), 13946 (2019).

[34]E. Y. L. Teo, G. A. M. Ali, H. Algarni, W. Cheewasedtham, T. Rujiralai, and K. F. Chong, Mater. Chem. Phys. **231**, 286–291 (2019).

[35]H. Abdi and L. J. Williams, Wiley Interdiscip. Rev.: Comput. Stat. **2**(4), 433–459 (2010).

[36]N. Bouhmala, paper presented at the 5th IIAI International Congress on Advanced Applied Informatics (IIAI-AAI), 2016.

[37]J. Irani, N. Pise, and M. Phatak, Int. J. Comput. Appl. **134**, 9–14 (2016).

[38]M. Hossin and M. N. Sulaiman, Int. J. Data Min. Knowl. Manage. Process. **5**(2), 11 (2015).

[39]J. Lotsch, D. Kringel, and T. Hummel, Chem. Sens. **44**(1), 11–22 (2019).

[40]A. J. Izenman, in *Modern Multivariate Statistical Techniques: Regression, Classification, and Manifold Learning*, edited by A. J. Izenman (Springer, New York, NY, 2008), pp. 237–280.

[41]T. Fushiki, Stat. Comput. **21**(2), 137–146 (2011).

[42]B. H. Menze, B. M. Kelm, R. Masuch, U. Himmelreich, P. Bachert, W. Petrich, and F. A. Hamprecht, BMC Bioinf. **10**(1), 213 (2009).

[43]C. Sinding, G. Coureaud, C. Chabanet, A. Chambault, N. Béno, T. Dosne, B. Schaal, and T. Thomas-Danguin, *Flavour Science* (Academic Press 2014), pp. 27–31.

[44]M. E. Frank, D. B. Fletcher, and T. P. Hettinger, Chem. Sens. **42**(7), 537–546 (2017).

[45]T. Thomas-Danguin, C. Sinding, S. Romagny, F. El Mountassir, B. Atanasova, E. Le Berre, A. M. Le Bon, and G. Coureaud, Front. Psychol. **5**, 504 (2014).

[46]L. M. Kay, T. Crk, and J. Thorngate, Behav. Neurosci. **119**(3), 726–733 (2005).

[47]Y. El-Sayed and T. J. Bandosz, Langmuir **21**(4), 1282–1289 (2005).

[48]M. Franz, H. A. Arafat, and N. G. Pinto, Carbon **38**(13), 1807–1819 (2000).

[49]A. Rajak, A. K. Singh, L. Roy, and A. Das, ChemNanoMat **8**(6), e202200082 (2022).

[50]E. M. D. Keegstra, A. L. Spek, J. W. Zwikker, and L. W. Jenneskens, J. Chem. Soc., Chem. Commun. **1994**(14), 1633–1634.

[51]Q. Yuan, Y.-P. Zhao, L. Li, and T. Wang, J. Phys. Chem. C **113**(15), 6107–6113 (2009).

[52]J. Wang, S. Rathi, B. Singh, I. Lee, H.-I. Joh, and G.-H. Kim, ACS Appl. Mater. Interfaces **7**(25), 13768–13775 (2015).

[53]H. Qi, J. Liu, J. Pionteck, P. Pötschke, and E. Mäder, Sens. Actuators, B **213**, 20–26 (2015).

[54]F. Balena and J. Fawcette, *Programming Microsoft Visual Basic 6.0* (Microsoft Press, Washington, 1999).

02 January 2025 11:54:10